

Comparison of Three Speed Loop Designs for a High Speed Nine-phase Permanent Magnet Synchronous Machine in More Electric Aircraft

Mi Tang
Power Electronics, Machine and Control Group
University of Nottingham
Nottingham, UK
mi.tang@nottingham.ac.uk

Tao Yang
Power Electronics, Machine and Control Group
University of Nottingham
Nottingham, UK
tao.yang@nottingham.ac.uk

Yuzheng Chen
Power Electronics, Machine and Control Group
University of Nottingham
Nottingham, UK
yuzheng.chen@nottingham.ac.uk

Mohammad Ilkhani
Power Electronics, Machine and Control Group
University of Nottingham
Nottingham, UK
mohammad.ilkhani@nottingham.ac.uk

Abstract – A high speed nine phase permanent magnet synchronous machine (PMSM) has been designed for more electric aircraft (MEA) for the sake of high power density and fault-tolerant capability. This paper addresses the speed loop design of the high speed PMSM by comparing three speed loop designs. For MEA, fast dynamic is not the primary demand, robustness against parameter variation and noise is the key requirement. For high speed machine, field weakening is not avoidable, therefore, maintaining the speed control during field weakening is also an important feature. This paper analyses the frequency response, stiffness and performance of the speed control with the three speed controllers, while the three controllers are tuned to provide the same control bandwidth. Simulation results validate the analysis. The pros and cons of each control design are summarised in the conclusion.

Index Terms—Speed loop design, nine-phase machine, more electric aircraft

I. INTRODUCTION

More electric aircraft (MEA) [1-3] and electrification has drawn more and more attention in recent decade. More electric power is preferred to improve the overall efficiency and reduce emissions of the aircraft. An integrated starter-generator system can save volume and weight [4]. To make the system even more compact, the machine is designed to achieve higher power and higher speed. What is more, to increase the fault-tolerant capability of the machine, it is also trendy to study multiphase machines for aircraft [5].

In order to maximize the fault tolerant capability, the nine phases of the machine are designed as triple electrically isolated three phases as in Fig. 1, namely three sectors. Since concentrate winding is used, the mutual inductances between phases and sectors are 25 times smaller than the self-inductances. Therefore, in healthy condition, the torque reference generated by the speed loop controller should be shared equally between the three sectors to maintain the

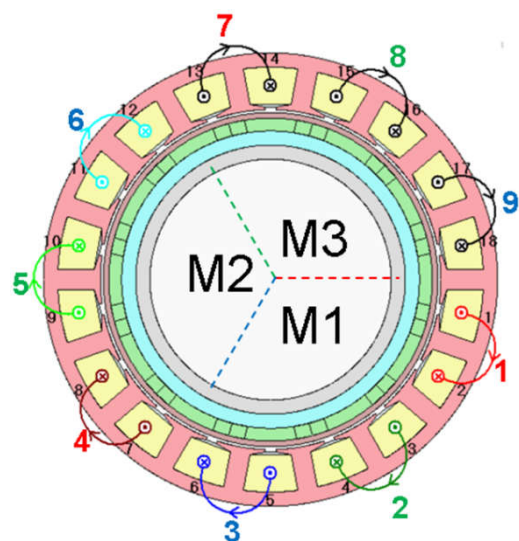


Fig. 1. Windings of the nine phase machine balance between the nine phases and avoid radial force.

Regarding the control of the high speed machine, a high performance current loop including field weakening is the foundation. After the high performance inner current and field weakening loops as in [6] have been designed, the outer control loop can be a speed control loop under the motoring mode or a dc voltage control loop under the generating mode. This paper focuses on the speed control.

The key requirement for the speed control in MEA is the robustness in terms of both performance and stability. A smooth transient response with no overshoot is preferred. Both the performance and stability should be maintained with imperfections such as measurement noise and parameter variations.

A vast of speed control methods have been proposed in literature. The classic control method is to use a proportional and integral (PI) controller as the feedback controller [7]. To improve the robustness against position measurement errors, adding a lowpass filter to the feedback path could be a quick fix. Alternatively, following the concept of the active disturbance rejection control [8,9,10], an observer-based

This project has received funding from the Clean Sky 2 Joint Undertaking under the European Union's Horizon 2020 research and innovation programme under grant agreement number 820913 and 821023.

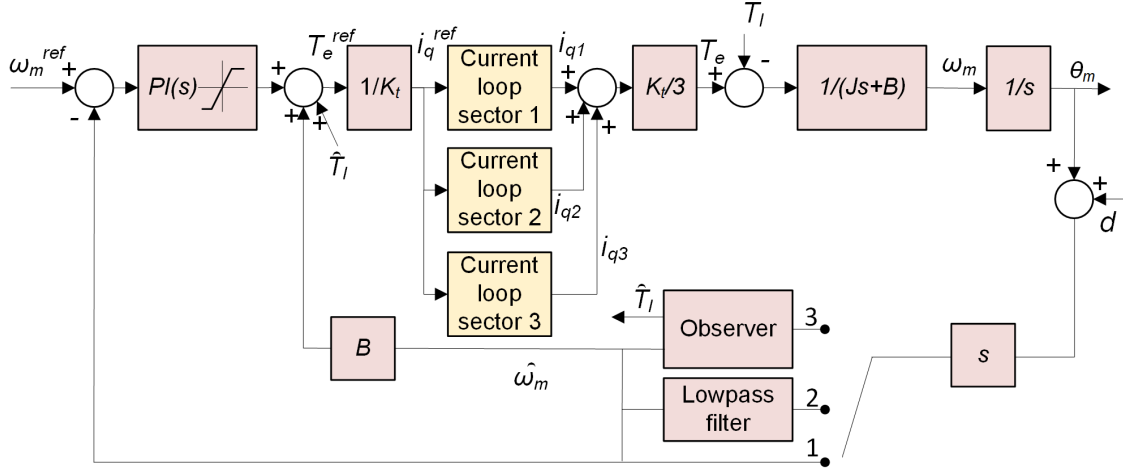


Fig. 2 The three intended speed loop control designs.

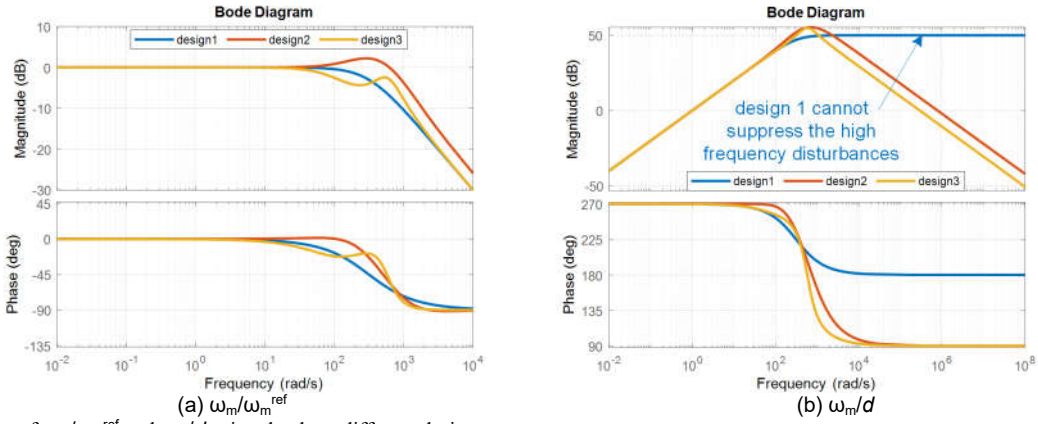


Fig. 3 Bode plots of ω_m/ω_m^{ref} and ω_m/d using the three different designs.

speed control loop can be developed. Other advanced control techniques such as deadbeat control and model predictive control [11] can improve the control dynamic, however, they will increase the dependence on parameters.

This paper compares the classic PI design, the PI with lowpass filter design and the observer-based design for the high speed multiphase PMSM in MEA. The frequency response, stiffness and performance of the speed control with the three speed controllers are analysed, while the three controllers are tuned to provide the same control bandwidth. Simulation results confirm that the simple PI with lowpass filter design can satisfy the requirements and achieve stable, smooth performance while maintaining low audible noise.

II. Design and tuning of the three speed loops

Considering the inner current loop as designed in [6] is at least 10 times faster than the outer speed loop, to simplify the design, the current loop of each three-phase sector is considered as a unity gain. The three intended speed loop designs are drawn in Fig. 2. Where, $J=0.00507\text{kgm}^2$, is the moment of inertia, $B=0.0004924\text{Nms/rad}$, is the friction factor. $K_t=0.7458\text{Nm/Apeak}$, is the torque constant of the machine. ω_m is the mechanical angular speed. “ref” denotes the reference signal. θ_m is the machinal rotor angular position. T_e is the electrical torque. T_l is the load torque. d is

the disturbance or noise, which can be for example the quantization error induced by the position sensors. In this paper, the resolution of the resolver used is 14 bits. All the intended speed controllers are designed in s-domain and discretised in z-domain using Forward Euler method.

A. Simple PI control

The simplest speed control design is to use one PI controller as defined in (1). Consequently, the transfer function of ω_m/ω_m^{ref} is derived as in (2).

$$PI_1(s) = K_p + \frac{K_i}{s} \quad (1)$$

$$G_1(s) = \frac{\omega_m}{\omega_m^{ref}} = \frac{K_p s + K_i}{J s^2 + (B + K_p) s + K_i} \quad (2)$$

Where, K_p and K_i are the proportional and integral gains of the PI, respectively.

To analyse the stiffness of the speed loop, the transfer functions of ω_m/d is derived in (3).

$$G_{1d}(s) = \frac{\omega_m}{d} = \frac{-K_p s^2 - K_i s}{J s^2 + (B + K_p) s + K_i} \quad (3)$$

K_p and K_i can be tuned following the pole placement method. To reduce overshoots in speed response, the closed loop transfer function G_1 is assumed to be a first order system. Consequently, K_p and K_i are solved as in (4).

$$G_1(s) = \frac{\omega_m}{\omega_m^{ref}} = \frac{K_p s + K_i}{J s^2 + (B + K_p) s + K_i} = \frac{\omega_0}{s + \omega_0} \\ \Rightarrow K_p = \hat{J} \omega_0, K_i = \hat{B} \omega_0 \quad (4)$$

Where, ω_0 is the control bandwidth of the speed loop. Since high dynamic is not the key requirement for MEA, $\omega_0=100\pi$ rad/s is selected. When the estimated inertia \hat{J} equals the real J and the estimated friction factor \hat{B} equals the real B , the closed loop is a first order system. The bode plots for G_1 and G_{1d} are drawn in Fig. 3.

B. PI control with lowpass filter

To attenuate the high frequency response in G_{1d} , a first order lowpass filter is added to the feedback loop, which is defined as in (5).

$$LP_1(s) = \frac{\omega_c}{s + \omega_c} \quad (5)$$

Consequently, the updated closed loop transfer function is given in (6).

$$G_2(s) = \frac{\omega_m}{\omega_m^{ref}} = \frac{K_p s^2 + (K_i + K_p \omega_c) s + K_i \omega_c}{J s^3 + (B + J \omega_c) s^2 + (B \omega_c + K_p \omega_c) s + K_i \omega_c} \quad (6)$$

The transfer function of ω_m/d is derived in (7).

$$G_{2d}(s) = \frac{\omega_m}{d} = \frac{-K_p \omega_c s^2 - K_i \omega_c s}{J s^3 + (B + J \omega_c) s^2 + (B \omega_c + K_p \omega_c) s + K_i \omega_c} \quad (7)$$

To achieve the same control bandwidth as G_1 , the three poles of (6) are placed at $s_1 = -\omega_0$, $s_{2,3} = -d_1 \omega_1 \pm j(1 - d_1)0.5\omega_1$. Where, s_1 is the dominate pole, d_1 and ω_1 are the damping and natural frequency of the pair of conjugate poles. The solution for parameters K_p , K_i and ω_c are given in (8).

$$\begin{aligned} \omega_c &= \omega_0 + 2d_1\omega_1 - \hat{B}/\hat{J} \\ K_p &= \frac{\hat{J}(2d_1\omega_0\omega_1 + \omega_1^2)}{\omega_c} - \hat{B}, K_i = \frac{\hat{J}\omega_0\omega_1^2}{\omega_c} - \hat{B} \end{aligned} \quad (8)$$

The bode plots of G_2 and G_{2d} are drawn in Fig.3.

C. Observer-based speed control

Since the stator position θ_m of the system is directly measured by the position sensor. Define the measured position as $\hat{\theta}_m = \theta_m + d$, states ω_m and T_l can be observed using the reduced-order observer in (9).

$$\begin{bmatrix} \hat{\omega}_m \\ \hat{T}_l \end{bmatrix} s = \begin{bmatrix} -\hat{B}/\hat{J} & -1/\hat{J} \\ 0 & 0 \end{bmatrix} \begin{bmatrix} \hat{\omega}_m \\ \hat{T}_l \end{bmatrix} + \begin{bmatrix} 1/\hat{J} \\ 0 \end{bmatrix} T_e + \begin{bmatrix} l_1 \\ l_2 \end{bmatrix} (\hat{\theta}_m s - \hat{\omega}_m) \quad (9)$$

Where, T_e is the torque reference calculated by the PI. $\hat{\omega}_m$ is the observed speed, \hat{T}_l is the observed load torque, l_1 and l_2 are the observer gains. Hence, the transfer functions of $\hat{\omega}_m/\hat{\theta}_m$ and $\hat{T}_l/\hat{\theta}_m$ are derived from (9) as in (10) and (11), respectively.

$$OB_{\omega}(s) = \frac{J l_1 s^2 - l_2 s}{J s^2 + (B + J l_1) s - l_2} \quad (10)$$

$$OB_{Tl}(s) = \frac{J l_2 s^2 + B l_2 s}{J s^2 + (B + J l_1) s - l_2} \quad (11)$$

According to the separation principle, the observer and the feedback controller can be tuned independently. To tune the observer, gains l_1 and l_2 can be calculated according to (11) by choosing the natural frequency ω_{ob} and damping dob of the observer. In this paper, ω_{ob} is set equal to the lowpass filter bandwidth ω_c in (5) and d_{ob} is set to one.

$$l_1 = 2d_{ob}\omega_{ob} - \hat{B}/\hat{J}, l_2 = -\hat{J}\omega_{ob}^2 \quad (11)$$

The speed loop transfer function ω_m/ω_{mref} with the observer is derived in (12).

$$G_3(s) = \frac{\omega_m}{\omega_m^{ref}} = \frac{JK_p s^2 + (BK_p + JK_p l_1) s - K_p l_2}{J^2 s^3 + (l_1 J^2 + 2BJ) s^2 + (B^2 - 2Jl_2 + JK_p l_1) s - Bl_2 - K_p l_2} \quad (12)$$

It is worth pointing out that the PI feedback controller is

only a P controller for the observer-based speed loop because the observer already has an integrator inside. The K_p of the P controller can be tuned assuming the observer is ideal and $OB_{\omega}=s$, $OB_{Tl}=0$, such that (12) is simplified as $K_p/(J_s + K_p)$. Therefore, the speed loop G_3 equals G_1 if (13) is hold:

$$K_p = \hat{J}\omega_0 \quad (13)$$

The transfer function of ω_m/d with observer is derived in (14).

$$G_{3d}(s) = \frac{\omega_m}{d} = \frac{(Jl_2 + BJl_1 - JK_p l_1) s^2 + K_p l_2 s}{J^2 s^3 + (l_1 J^2 + 2BJ) s^2 + (B^2 - 2Jl_2 + JK_p l_1) s - Bl_2 - K_p l_2} \quad (14)$$

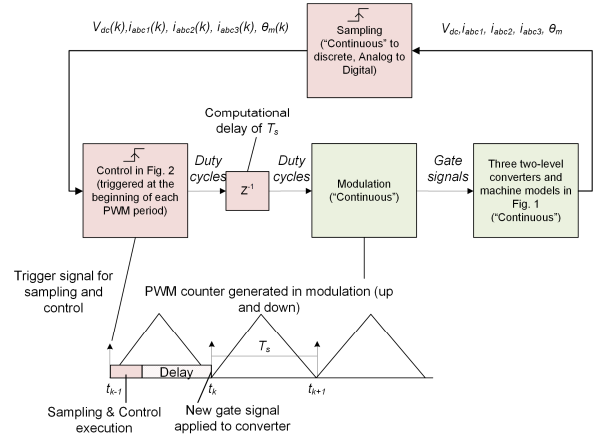


Fig. 4 Simulation model.

The bode plots of G_3 and G_{3d} are drawn in Fig.3.

III. SIMULATION RESULTS

Simulation model as in Fig. 4 has been built in Matlab/Simulink to verify the performance of the three speed loop designs.

In Fig. 4, the nine-phase machine is modelled in alpha-beta frame. Three two-level converters are modelled with the switching effect but no deadtime. The controller is triggered at the beginning of each PWM cycle. The speed control is as shown in Fig. 2, while the inner current loop including field weakening is implemented as in [6]. The sampling and switching period T_s are 40kHz.

During the test, the speed reference steps from 0 krpm to 20 krpm in 5 steps. The load torque is set to half of the rated torque. The speed error and current responses are shown in Fig. 5.

As shown in Fig. 5, there are two issues with the design 1: 1) Since there is no filter at the speed feedback, the speed feedback is noisy due to the quantization error. This matches the bode plot of ω_m/d in Fig. 3. 2) There are some steady-state errors in the speed response since the integral gain K_i calculated from (4) is too small due to small value of B . The steady state error can be reduced by increasing the parameter K_i .

For the design 2, thanks to the lowpass filter used, the noise in the speed feedback is massively reduced. Although the dominate pole in design 1 and design 2 are the same, the K_i calculated from (8) is much larger than it calculated from

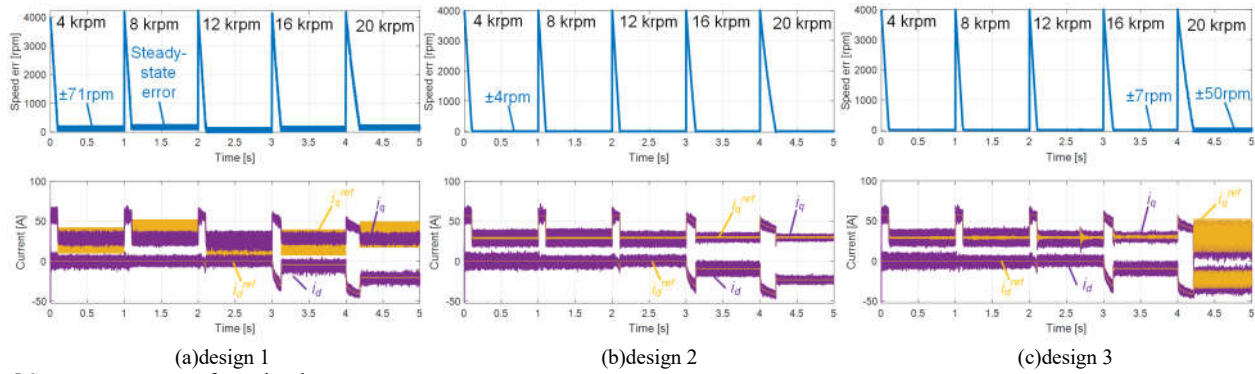


Fig. 5 Step response error of speed and current responses.

(4). Therefore, there is also no steady-state error in Fig. 5b. The amplitude increases in i_d when the speed is above 12 krpm show that the field weakening loop is working.

Regarding the design 3, it performs better than the design 1 but worse than the design 2. Although as analysed in Fig. 3b, the design 3 also has strong attenuation effect for high frequency disturbance, i.e. the quantization error in this case, however, the current reference can be very noisy at high speed due to unmodelled switching noise and unmodelled interaction between the field weakening loop and the speed loop. Such switching noise is normally handled by the current loop and thus not considered in the speed loop design. Nevertheless, such current noise will contribute the audible noise, so it is necessary to keep the current reference as “clean” as possible.

IV. CONCLUSIONS

This paper compares and evaluates three speed control design for a high speed multiphase PMSM in MEA. Results show that the PI with lowpass filter design satisfies well the robustness requirement of MEA. It achieves smooth transient with no overshoots during reference transients while maintaining low audible noise. It is not only robust against parameter variation but also robust against disturbances.

ACKNOWLEDGMENT

This project has received funding from the Clean Sky 2 Joint Undertaking under the European Union’s Horizon 2020 research and innovation programme under grant agreement number 820913 and 821023.

REFERENCES

- [1] P. Wheeler and S. Bozhko, "The more electric aircraft: Technology and challenges," IEEE Electrification Magazine, vol. 2, no. 4, pp. 6-12, 2014.
- [2] X. Lang, T. Yang, C. Li, H. B. Enalou, S. Bozhko, and P. Wheeler, "A Dual-Channel-Enhanced Power Generation Architecture With Back-to-Back Converter for MEA Application," IEEE Transactions on Industry Applications, vol. 56, no. 3, pp. 3006-3019, 2020.
- [3] S. Bozhko et al., "Development of aircraft electric starter-generator system based on active rectification technology," IEEE Transactions on Transportation Electrification, vol. 4, no. 4, pp. 985-996, 2018.
- [4] Mao, Shuai, et al. "Sensorless Starting Control of Brushless Synchronous Starter/Generators for the Full-Speed Range." IEEE Transactions on Power Electronics 35.8, 8347-8360, 2019.
- [5] Zhang, Zhuoran, et al. "Overview and analysis of PM starter/generator for aircraft electrical power systems." CES Transactions on Electrical Machines and Systems 1.2, 117-131, 2017.
- [6] M. Tang *et al.*, "Optimised current loop design for a high speed nine-phase permanent magnet synchronous machine in more electric aircraft: A case study," 2021 IEEE Transp. Electrification Conf. Expo, ITEC 2021, pp. 665–671, 2021.
- [7] Villani, Marco, et al. "High reliability permanent magnet brushless motor drive for aircraft application." IEEE transactions on industrial electronics 59.5, 2073-2081, 2011.
- [8] Diab, Ahmed M., et al. "Stable and Robust Design of Active Disturbance-Rejection Current Controller for Permanent Magnet Machines in Transportation Systems." IEEE Transactions on Transportation Electrification 6.4, 1421-1433, 2020.
- [9] L. Qu, W. Qiao and L. Qu, "An Extended-State-Observer-Based Sliding-Mode Speed Control for Permanent-Magnet Synchronous Motors," in IEEE Journal of Emerging and Selected Topics in Power Electronics, vol. 9, no. 2, pp. 1605-1613, 2021.
- [10] L. Yan, F. Wang, M. Dou, Z. Zhang, R. Kennel and J. Rodríguez, "Active Disturbance-Rejection-Based Speed Control in Model Predictive Control for Induction Machines," in IEEE Transactions on Industrial Electronics, vol. 67, no. 4, pp. 2574-2584, 2020.
- [11] T. Tarczewski and L. M. Grzesiak, "Constrained State Feedback Speed Control of PMSM Based on Model Predictive Approach," in IEEE Transactions on Industrial Electronics, vol. 63, no. 6, pp. 3867-3875, 2016.